



**HAL**  
open science

# Binding Sites of Bicarbonate in Phosphoenolpyruvate Carboxylase

Nicolas Chéron

► **To cite this version:**

Nicolas Chéron. Binding Sites of Bicarbonate in Phosphoenolpyruvate Carboxylase. *Journal of Chemical Information and Modeling*, 2024, 64 (8), pp.3375-3385. 10.1021/acs.jcim.3c01830 . hal-04559565

**HAL Id: hal-04559565**

**<https://hal.science/hal-04559565v1>**

Submitted on 25 Apr 2024

**HAL** is a multi-disciplinary open access archive for the deposit and dissemination of scientific research documents, whether they are published or not. The documents may come from teaching and research institutions in France or abroad, or from public or private research centers.

L'archive ouverte pluridisciplinaire **HAL**, est destinée au dépôt et à la diffusion de documents scientifiques de niveau recherche, publiés ou non, émanant des établissements d'enseignement et de recherche français ou étrangers, des laboratoires publics ou privés.

# Binding Sites of Bicarbonate in Phosphoenolpyruvate Carboxylase

*Nicolas Chéron\**

PASTEUR, Département de chimie, École normale supérieure, PSL University, Sorbonne  
Université, CNRS, 75005 Paris, France

**Corresponding Author:**

\*Email: [nicolas.cheron@ens.psl.eu](mailto:nicolas.cheron@ens.psl.eu)

**ABSTRACT:** Phosphoenolpyruvate carboxylase (PEPC) is used in plant metabolism for fruit maturation or seed development, as well as in the C4 and crassulacean acid metabolism (CAM) mechanisms in photosynthesis where it is used for the capture of hydrated CO<sub>2</sub> (bicarbonate). To find the yet unknown binding site of bicarbonate in this enzyme, we have first identified putative binding sites with non-equilibrium molecular dynamics simulations, and then ranked these sites with alchemical free energy calculations with corrections of computational artefacts. 14 pockets where bicarbonate could bind were identified, with three having realistic binding free energies with differences with the experimental value below 1 kcal/mol. One of these pockets is found far from the active site at 14 Å, and is predicted to be an allosteric binding site. In the two other binding sites, bicarbonate is in direct interaction with the magnesium ion; neither sequence alignment nor the study of mutant K606N allowed to discriminate between these two pockets and both are good candidates as the binding site of bicarbonate in phosphoenolpyruvate carboxylase.

**KEYWORDS:** Molecular dynamics, Binding free energy, Enzymes, Photosynthesis, Carbon dioxide.

## Introduction

In the context of an ever increasing global population (expected to grow from 7 billion in 2011 to 9 billion in 2050<sup>1</sup>), there will be a need for new resources. Improving crop yields is a promising solution, since photosynthesis provides humans with many resources, from food to cloth fibers, from building wood to sources of clean energy. The rate-limiting step of photosynthesis has long been considered to be the enzyme Rubisco<sup>2</sup>, which catalyses the reaction between carbon dioxide (CO<sub>2</sub>) and the substrate ribulose 1,5-bisphosphate (RuBP). However, the picture of a single enzyme which would be the bottleneck of photosynthesis and of plant growth is now questioned, and is probably true only in conditions of high light, high temperature, and for C<sub>3</sub> organisms<sup>3,4</sup>. Indeed, when other enzymes of the Calvin-Benson<sup>5</sup> cycle such as sedoheptulose-1,7-bisphosphatase (SBPase) are overexpressed in different organisms, the photosynthetic rates are increased which leads to more biomass<sup>6-8</sup>, suggesting that Rubisco is not the bottleneck. In contrast, the overexpression of Rubisco in rice can lead to a decrease of the CO<sub>2</sub> assimilation rate at 25°C (and an increase at 40°C)<sup>9</sup>. Moreover, the estimated rate of transformations of metabolites from ribulose-5-phosphate-3-epimerase (RPE) is estimated to be slightly lower to the one from Rubisco<sup>10</sup>. These results are in line with the statement that despite a slow kinetic rate, “Rubisco is not really so bad”<sup>11,12</sup>. Thus, the reality is more complex than a textbook description of a single bottleneck enzyme.

97% of plant varieties belongs to the C<sub>3</sub> family, where CO<sub>2</sub> is simultaneously captured and integrated in the organism *via* Rubisco<sup>2</sup> during the Calvin-Benson cycle<sup>5</sup>. The remaining 3% of varieties belong to the C<sub>4</sub> and crassulacean acid metabolism (CAM) families, where at first the enzyme PEP carboxylase (PEPC) captures the carbon through the catalysis of the reaction between hydrated CO<sub>2</sub> (bicarbonate, HCO<sub>3</sub><sup>-</sup>) and phosphoenolpyruvate (PEP) to form oxaloacetate (see

Figure 1). This metabolite is then converted and transported to another cell where CO<sub>2</sub> is released and incorporated in the organism by Rubisco during the Calvin-Benson cycle<sup>2</sup>. Separating the capture of CO<sub>2</sub> by PEPC from its integration in the organism by Rubisco in two different cells prevents a costly side reaction also catalysed by Rubisco when in contact with O<sub>2</sub> (photorespiration), and C<sub>4</sub> plants are then more efficient than C<sub>3</sub> plants for carbon capture, especially in hot environments<sup>13,14</sup>. Even if the C<sub>4</sub> or CAM mechanisms are found in only 3% of plant varieties, C<sub>4</sub> plants represent 23% of terrestrial carbon fixation<sup>2</sup>, including plants of huge importance such as *sugarcane*, *maize* (the most grown cereal in the world<sup>15</sup>), *millet* (one of the only edible plant that can grow in arid regions) or *switchgrass* (a serious candidate for developing the production of biofuels<sup>16</sup>). The reaction catalysed by PEPC is thus at a key position for food and resource productions, and PEPC may be involved in the overall control of carbon flux<sup>4,17</sup>. Moreover, in addition to photosynthesis in C<sub>4</sub> plants, PEPC is used in all plants metabolism for functions such as fruit maturation, seed development or amino acid synthesis and is thus a central enzyme for the plant kingdom<sup>18</sup>.

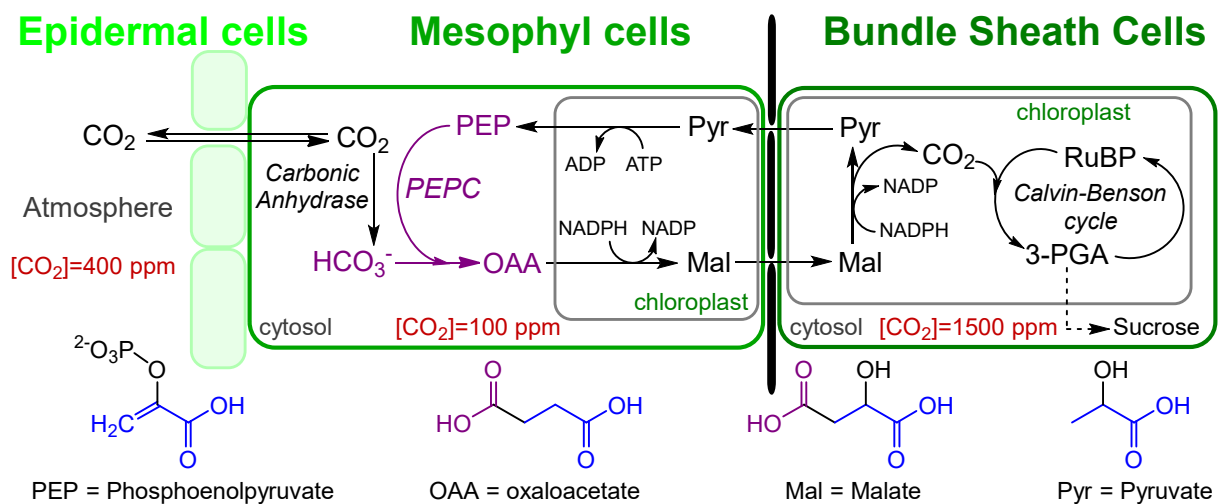


**Figure 1.** Simplified mechanism of carbon capture and fixation in C<sub>4</sub> plants<sup>2</sup>.

We propose herein to focus on the enzyme PEPC, aiming to provide new information that will be useful for future engineering. Indeed, plant engineering was mainly focused towards Rubisco for a long time (with limited success), and the paradigm has changed towards an increasing interest on the C4 mechanism (e.g., the C4 Rice Project<sup>19</sup>) where PEPC sits at the beginning of carbon flux. In addition to improve plant growth, PEPC has also been used in the development of new-to-nature CO<sub>2</sub> fixation pathway<sup>20</sup>. Thus, a full understanding of this enzyme at the molecular level is needed, whereas the mechanism of carbon-capture by PEPC in C4 plants is still not fully elucidated: (1) global motions of the enzyme are still not understood, such as the movements of loop II (residues 761-768 in maize numbering) during the catalytic cycle. This loop is supposed to serve as a lid to protect the active site and to exist in two conformations<sup>21</sup>, however it was found fully complete in only four of the 17 published crystallographic structures of PEPC, and always in the same conformation. (2) The understanding of regulation in PEPC is still not complete, for example the role of phosphorylation at a molecular level and its consequences on the enzyme's structure<sup>21</sup>. (3) The chemical mechanism of the enzyme is supposed to be a three-step mechanism<sup>21-23</sup>, however extracting microscopic information specific to each step from the macroscopic measurements has proven to be difficult and the free energy profile of the reaction is still not known. Thus, the concerted or sequential characters of the different steps, as well as the identity of the rate-determining step, are unknown. Since experimental approaches have not yet been able to answer these questions, one could rely on computational techniques. However, crucial details on PEPC are still lacking and currently preclude the use of simulations to answer these questions, starting with the localisation of one of the two substrates (bicarbonate), which will be the focus of this article.

To identify the binding site of a ligand, structural approaches are the optimal choice. To date, 17 crystallographic structures of PEPC are available on the PDB database. Among them, 12 are currently described in a published article (see Table SI-1). None of these studies focused on bicarbonate, and as a consequence bicarbonate was not present in the medium during crystal growth for all these structures. Moreover, we didn't find any structural NMR or CryoEM study performed on PEPC. Thus, no information on the bicarbonate binding site could be inferred from structural studies. Enzymatic assays are another way to get information on ligand binding. Analyses of the Brenda and Sabio-RK databases provided 37 references that provided Michaelis constant ( $K_M$ ) for bicarbonate. Most of these studies focused on a single enzyme, while others compared isozymes or different growth medium: in neither case these studies could be used to describe the binding of bicarbonate. Only a few reports describe mutants of an enzyme, which allows direct comparison of the role of a given residue. Kai *et al.*<sup>24</sup> observed that mutations of Arg703 and Arg704 in *E. coli* (corresponding to Arg763 and Arg764 in maize numbering) affects  $K_M$ , suggesting that these residues are important for bicarbonate binding (respectively 0.10 mM, 0.55 mM and 6.5 mM for wildtype and mutants R703G and R703G/R704G). However, these residues are in a loop that is suspected to adopt a close conformation to protect the active site (loop II in cyan in Figure 2), and upon the mutations a side-reaction involving water molecules from solvent occurs; thus, the change of  $K_M$  could solely be due to the change of loop conformation and of global environment, and not be directly linked to bicarbonate binding. Lys606 (in maize numbering) was found to influence bicarbonate binding: in maize, Dong *et al.*<sup>25</sup> observed an increase of  $S_{0.5}$  from 0.1 mM for wildtype to 2.5, 2.1 and 0.2 mM for respectively the mutants K606N, K606E and K606R. Similarly, Gao *et al.*<sup>26</sup> found an increase of  $K_M$  from 0.061 mM in wildtype to 0.114 and 0.602 mM in mutants K600R and K600T in *Flaveria trinervia* (where K600

corresponds to K606 in maize). Yano *et al.*<sup>27</sup> focused on Arg587 in *E. coli* (which corresponds to Arg647 in maize numbering) and showed that it affects bicarbonate binding with  $S_{0.5}$  increasing from 0.25 to 24 mM between wildtype and mutant R587S. DiMario *et al.*<sup>28</sup> looked at residue 774 in *Flaveria trinervia* (780 in maize numbering) and found an increase in  $K_M$  in the C4 enzyme from 26.6 to 38.6  $\mu$ M between wildtype and mutant S774A. However, Ser780 is located at 16 Å from the  $Mg^{2+}$  in the active site and behind loop II, and it is very likely that it is more involved in a structural role for loop II motions, than in bicarbonate binding. A very weak effect of Lys829 in *Flaveria trinervia* was observed by Gao *et al.*<sup>29</sup>, with  $K_M$  decreasing from 0.072 to 0.054 mM between wildtype and mutant K829G. However, the same team reported a different value of 0.061 mM for wildtype at the same pH in another article<sup>26</sup>, and the influence of residue Lys829 is thus probably not significant. The binding site of aspartate –a negative allosteric ligand– was also studied for PEPC of three bacteria, and no studied mutations affected  $K_M$  of bicarbonate significantly<sup>30,31</sup>. Thus, only two residues were found to be possibly involved in bicarbonate binding: Lys606 and Arg647 (in maize numbering). Unfortunately, that doesn't provide enough data to firmly conclude on the localisation of bicarbonate. Thus, we propose herein to address the question of bicarbonate binding site, which will then allow to computationally study PEPC and get more insights on this important enzyme.

Some small featureless ligands, such as  $CO_2$ , are sometimes said to be “slippery” because they can't bind to an enzyme and don't form a Michaelis complex with Rubisco<sup>32</sup>. However, Michaelis constants can be measured for bicarbonate in PEPC, which is consistent with the fact that the ligand is negatively charged and that there are several positively charged residues in the active site of PEPC. Thus, we envisioned that it should be possible to identify an effective binding site for bicarbonate in PEPC. In the current article, which is the first of a series on PEPC, we seek to help



answering the question: “Where does bicarbonate bind in PEP Carboxylase?”. Since to date no experimental techniques answered this question, we relied on computational tools and in particular on molecular dynamics (MD) simulations to provide some insights on this question. Some computational tools are designed to identify binding sites, such as FTsite, DeepSite, FPocket or CASTp to name a few that are still available<sup>33–36</sup>. However, these tools couldn’t be used here because bicarbonate is too small to provide significant results.

## **Presentation of PEPC**

The PEP Carboxylase (PEPC, E.C. 4.1.1.31) has been known for decades and has already been reviewed<sup>21,37–40</sup>. Its structure was first resolved in 1999 for bacteria (*E. coli*<sup>24</sup>) and in 2002 for plants (*Zea mays*<sup>23</sup>). It is a large enzyme (870 to 1150 residues depending on the organism<sup>21</sup>) whose functional form is a tetramer. The contact surface areas between one monomer and its two neighbors are 450 and 3000 Å<sup>2</sup>, and the structure is thus better described as a dimer of dimers<sup>21</sup> (see Figure 2 for the dimer and Figure SI-1 for the tetramer). In the current article, we focused on a dimer of the enzyme from *Zea mays* to save computational time. In 2002, the structure 1JQN was resolved with Mn<sup>2+</sup> as an analog to Mg<sup>2+</sup> and the ligand 3,3-dichloro-2-phosphonomethyl-acrylic acid (DCDP) as an analog to PEP, which allowed to locate the position of these ligands. In their vicinity, one can find three important loops: (i) the loop II (residues 761-768 in maize numbering) which is supposed to be a mobile loop that is closed during the catalytic cycle<sup>21</sup>; (ii) the loop I (residues 640-649) which can change of conformation upon aspartate binding to displace Arg647 away from the active site<sup>21</sup>; (iii) the loop 174-184 which can change of conformation upon glucose-6-phosphate (G6P) binding to place His177 within the active site<sup>21</sup>. Aspartate and G6P serve respectively as allosteric inhibitor and activator, and in addition neutral amino acids such as

glycine can also serve as allosteric activators (see Figure 2 for the active site and the binding site of allosteric effectors). Thus, PEPC is an enzyme that is highly regulated, which is usually a sign of importance for the organism. The proposed chemical mechanism and the phosphorylation mechanism are not discussed here and the interested reader is invited to consult reviews on PEPC<sup>21,37-40</sup>.

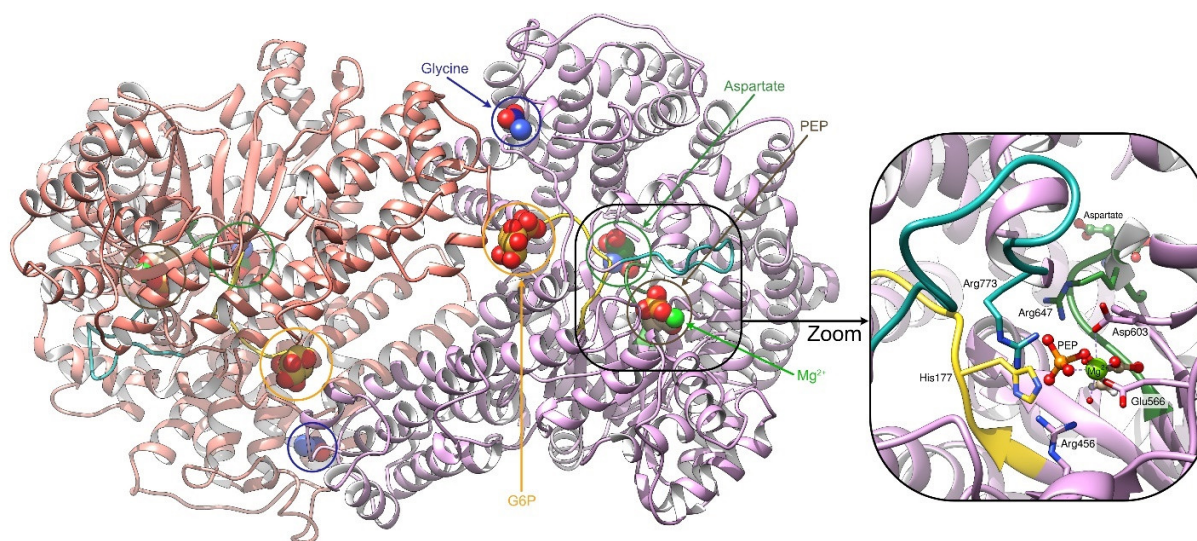


**Figure 2.** Dimer of PEP Carboxylase and zoom on active site. Ligands in the dimer are in spheres in the full enzyme, loop II is in cyan, loop 174-184 which moves upon glucose-6-phosphate binding is in gold, loop 640-649 which moves upon aspartate binding is in green.

## Building the system

This article is the first computational study performed on full PEPC (with the exception of some docking studies performed previously<sup>41-43</sup>) and is the first of a series, we will thus describe in some details the building of the system. We provide in Table SI-1 an analysis of the 17 available crystallographic structures. We started with the structure 5VYJ<sup>42</sup> (from *Zea mays*) resolved in 2018 at 3.3Å of resolution, since it is the first structure with the complete loop 761-768. However, loop

126-140 is missing in 5VYJ, we thus used the UCSF Chimera's interface to Modeller to build missing parts of the enzyme<sup>44,45</sup>: one adjacent residue was allowed to move, five models were generated, and the loop modeling protocol was set to DOPE<sup>46</sup>. To decide which model to choose, we aligned the structure 6U2T with completed models of 5VYJ and picked the model the closest to the loop 126-140 from 6U2T (from visual inspection). Residues 932/934/935 are also missing in 5VYJ: they were modelled in a similar way, and the model with the best DOPE score was retained. We then aligned the structure 1JQN<sup>23</sup> (from *E. coli*) with 5VYJ to obtain the position of the two analogs  $Mn^{2+}$  and DCDP, which were then manually modified to  $Mg^{2+}$  and PEP. From 5VYJ, acetate ions were removed and glycines (an allosteric activator) that are bound in their actual binding sites were kept (i.e. one glycine molecule was removed out of the five that were resolved). The build structure did not contain glucose-6-phosphate (G6P, an allosteric activator) nor aspartate (an allosteric inhibitor). Finally, we kept chains A and B for further investigations.

All structures were solvated in rhombic dodecahedron boxes, with a distance of at least 8 Å between two replicas of the system. This corresponds to edges of a triclinic box of roughly 155, 155 and 110 Å, which are filled by ~72000 water molecules (for a total of ~250000 atoms). Under physiological conditions, the enzyme is surrounded by a media with concentrations of 0.1 mM of bicarbonate, 3 mM of PEP, 0.4 mM of free  $Mg^{2+}$ , and 20 mM of L-malate<sup>47</sup>. These concentrations correspond to respectively 0.1 molecule of bicarbonate in the box, 3.9 molecules of PEP, 0.5 magnesium(II) and 25.9 molecules of malate: we have thus included in the simulation box 0 free bicarbonate, 4 free PEP, 0 free magnesium(II) and 26 free malate. In addition to these molecules, we have neutralized the charge with sodium ions and added a concentration of 0.1 M of sodium chloride (leading to respectively ~250 sodium and ~150 chloride). Computational details are described at length in SI.

## Identification of binding sites

To identify the binding site of bicarbonate in an unbiased way, we started by pushing bicarbonate inside the protein with steered MD simulations. Starting conformations were manually created by placing bicarbonate at 50 different localisations around PEPC: 35 with the axis between bicarbonate and PEP aligned with the loop II, and 15 with this axis aligned with the  $\beta$ -barrel of PEPC (see Figure 3 and Figure SI-3). For each starting position, we performed two steered MD simulations along different reaction coordinates: (i) the distance between C of bicarbonate and P from PEP, (ii) the distance between C of bicarbonate and C2 from PEP (which is the  $sp^2$  carbon bound to the carboxyl and the phosphate). During these simulations, the distance between bicarbonate and PEP decreased at a rate of  $1.0 \text{ \AA/ns}$  and was restrained with a force constant of  $k=10000 \text{ kJ/mol/nm}^2$ . The initial distances ranged from 22 to  $56 \text{ \AA}$  and the simulation length was chosen so that the final distance reached  $\sim 4 \text{ \AA}$ ; the steered MD simulations lasted from 15 to 58 ns. To get insights into the penetration process, free energy profiles along the reaction coordinate were computed and results are discussed in SI. At the end of these 100 simulations, bicarbonate was found at different localisations in the active site, but bicarbonate was still not in actual binding sites (Figure SI-6).

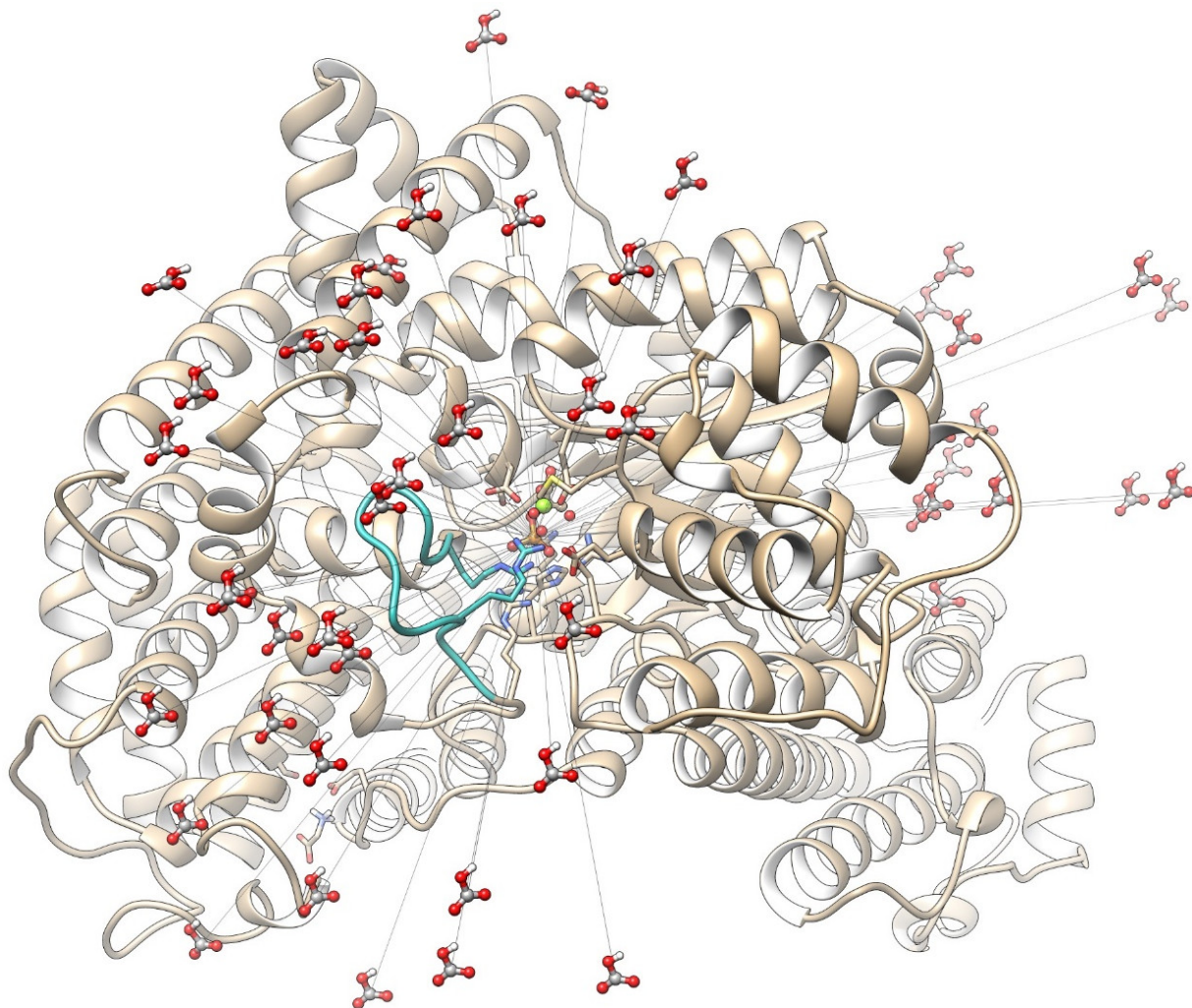


**Figure 3.** Super-imposition of starting positions of bicarbonate before steered MD simulations (in each simulation, only one bicarbonate was present). The lines joining C of bicarbonate and P of PEP are shown in grey. Loop II is in cyan. Additional images are available in Figure SI-3.

Following the steered MD simulations, 100 ns-long free MD simulations without any constraint were performed to let bicarbonate sample the active site region: we observed that during these simulations the ligand ended up in 14 different pockets, which we labelled P1 to P14 and which are shown in Figure 4 as well as in Figure SI-7. A localisation in the active site is considered as a pocket when bicarbonate stayed there at least 50 ns (a more thorough discussion on the pockets is

proposed in SI, where we describe how we identified and validated them). Eight of the free simulations were extended to 200 ns because a change of bicarbonate position occurred during the second half of the simulation (after 50 ns), thus bicarbonate had not reached a pocket according to our definition. Two pockets were populated each in a single simulation, whereas one of the pockets (P1) was populated 31 times (see Table SI-4). During 10 simulations, bicarbonate unbound from the protein and diffused in the solvent. We observed that in some of these 10 simulations, bicarbonate was first in pocket P1 before unbinding: this provided contradictory results, since on one hand pocket P1 is the most populated pocket which seemed to indicate it is the most favourable pocket with the lowest binding free energy, and on the other hand bicarbonate could escape from pocket P1 meaning that the interactions were not strong enough to retain bicarbonate. During these free MD simulations, we observed barely no exchange between pockets which means that thermodynamic equilibrium had not been reached and that the absolute binding free energy in each pocket had to be computed to compare and rank all of them. We first tried to extract the binding free energy from a physical path by pulling bicarbonate outside the active site and computing the free energy profile along that path with umbrella sampling simulations. This approach was not conclusive (see details in SI), and we have thus decided to perform alchemical transformations coupled with free energy perturbations to accurately compute the absolute binding free energies in each pocket.

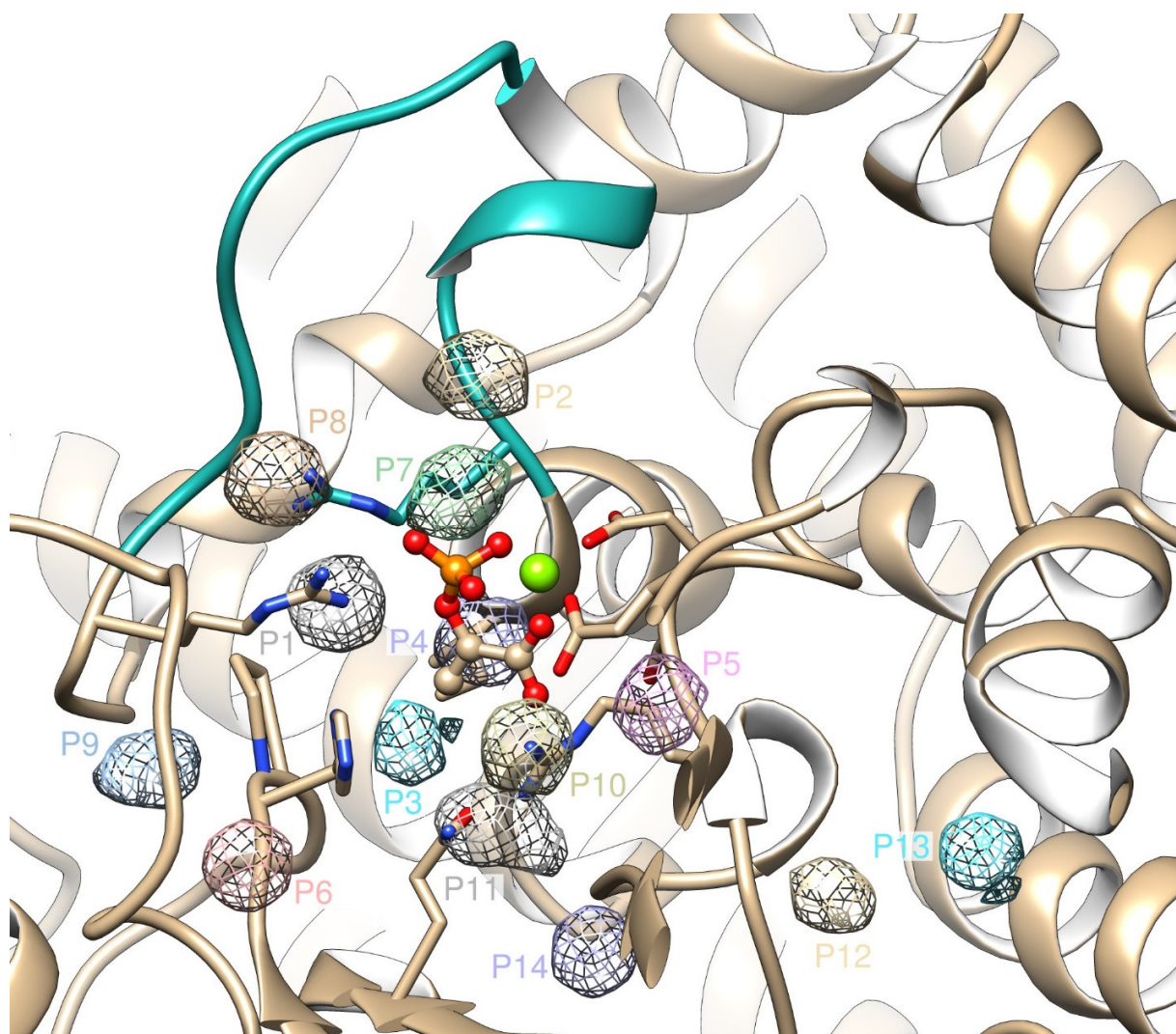


**Figure 4.** Identified binding sites of bicarbonate after alignment. The densities of bicarbonate in simulations representative of each pocket were analysed with GROmaps<sup>48</sup> and are here represented as isosurfaces with all the same threshold. PEP is in ball and stick,  $Mg^{2+}$  is in green, loop II is in cyan. Additional images are available in Figure SI-7.

### **Alchemical transformations with free energy perturbations**

Since the free energy is a state function, the followed path is not relevant to compute the difference of free energy between two states. Thus, one can change the chemical nature of compounds and

transfer them through a non-chemical way from bulk solvent to the binding site of an enzyme to compute the binding free energy: this kind of approach is called *alchemical transformations*. It is nowadays widely used, especially for drug design, and it has been numerously reviewed<sup>49-55</sup>. Using this approach, we have decomposed the binding free energy with a thermodynamic cycle where four terms must be computed independently: (1) the desolvation of the ligand, (2) the cost of adding restraints, (3) the binding free energy with restraints, (4) the gain in removing the restraints. We will briefly discuss these terms here; they are discussed at length with more computational details in SI. The cost of adding restraints can be obtained with an analytical function since it is only linked to the *ratio* of occupied volume with and without the restraints. The gain in removing the restraints is usually null for good ligands in good pockets and is often omitted. However, since we are here investigating pockets that can be not favourable, the gain in removing the restraints was also computed explicitly by progressively changing the amount of restraints. The desolvation of the ligand and the binding free energy with restraints were obtained through alchemical transformations of the ligand with free energy perturbations (FEP): in this kind of calculations, a series of simulations in which a coupling parameter  $\lambda$  varies are performed (for example,  $\lambda$  goes from 0 to 1 by steps of 0.1). If the variations of  $\lambda$  are small enough, one can compute the difference of free energies between two neighbour states, and by cumulating the differences one can get the difference of free energies between the two end states. This was used to make the ligand disappear from bulk solvent (desolvation free energy) and then appear in the enzyme (binding free energy). We have here used 21 alchemical windows to switch off the intermolecular interactions between bicarbonate and its environment (solvent or PEPC). To actually compute the differences of free energies, two approaches can be used efficiently: Thermodynamic Integration (TI) or the Bennett Acceptance Ratio (BAR). We have compared the



two, and for the later we have used the more modern multistate BAR (MBAR)<sup>56</sup>. The python packages `alchemlyb` and `pymbar`<sup>56</sup> were used to process the simulations and perform the calculations.

Assessing the convergence of FEP calculations is crucial to provide significant results, and is again discussed at length in SI. The convergence analysis was performed with MBAR, before comparing the results with those from TI. For each set of simulations (i.e. for each starting point used for the alchemical transformations), we have first performed a forward/backward analysis to assess the needed length of the simulations to reach convergence. The goal was that the first half and the second half of the used data provide comparable results, meaning that this set of simulations is converged with that amount of data. The data that were used for this analysis were extracted from the end of the simulations with an increasing size of the time bloc (i.e. last 10 ns, last 11 ns, last 12 ns, and so on), and we aimed at the longest time bloc that provides a difference between the two halves below  $1 k_B T$ <sup>54</sup>. If the objectives could not be reached, the simulations were extended by 5 ns. At the end, all simulations for the binding free energy with restraints lasted between 20 and 40 ns, used at least 10 ns of data, and the computed errors from both MBAR and TI were on average 0.03 kcal/mol, ranging from 0.02 to 0.04 kcal/mol. We have then verified that the phase space overlaps between each neighbouring windows were high enough, and found that they are 23% on average on the first off-diagonal matrix, with a lowest value of 7% (whereas the recommended lower acceptable value is 3%<sup>54</sup>).

When alchemical transformations are performed on charged species, they must be corrected from computational artefacts (called finite-size effects) prior comparisons with experimental data. Indeed, since the total charge of the system changes between the two end states, the background potential in the simulation boxes changes as well, which influences the potential energies, hence

the computed free energies. Different approaches exist to correct these artefacts<sup>57,58</sup>, and we relied on the one proposed by Rocklin *et al.*<sup>57</sup> where four effects are corrected: (1) the electrostatic interactions between the reference box, the periodic replicas and the neutralizing background, (2) the undersolvation due to the solutes in the periodic replicas, (3) the solvent-excluded volume of the solutes and the fact they are not point charges, (4) the difference of reference for the electrostatic potential between simulations and bulk experiments. The corrections must be performed for both the desolvation of the ligand and the binding process, and they are applied *a posteriori* through equations that are given in SI. For each pocket, 50 different snapshots were extracted every 1 ns from the free MD simulations, and the computational artefacts were computed on each snapshot. Standard deviations between snapshots from a pocket are always low (below 0.07 kcal/mol, see Table SI-11), which illustrates that a single snapshot could have been used to correct finite-size effects. Moreover, we observed that the correction values between the 14 pockets are all comparable (range of 0.2 kcal/mol).

To compare the binding free energies in each pocket, several independent replicas were used for some pockets. In such cases, the starting points for the replicas were extracted every 10 ns from the end of the free MD simulations (e.g. at 100 ns, 90 ns, 80 ns, and so on). Since FEP calculations are intensive in terms of computational resources, we have followed the following procedure: (i) we first performed the full calculations with three replicas for the first six identified pockets (P1 to P6). The lowest binding free energy was  $\Delta G = -6.7$  kcal/mol with standard deviations between 0.5 and 2.7 kcal/mol. For pockets with meaningful binding free energies (i.e. pockets P3 and P5 with -4.8 and -6.7 kcal/mol), the less favourable binding free energy of the different replicas was -3.4 kcal/mol. (ii) We then performed calculations for one replica in each remaining pocket. In these eight pockets, three had a binding free energy lower than -3.0 kcal/mol in the first

calculations (P7, P8 and P13), and we thus performed two additional replicas for them. For P8, the average binding free energy of the three replicas was  $-2.1 \pm 0.5$  kcal/mol, and we didn't investigate it further. For pockets P7 and P13, the average binding free energies of the three replicas were  $-7.2 \pm 1.4$  and  $-6.6 \pm 1.0$  kcal/mol respectively, and two extra replicas were performed to lower the standard error. (iii) Two additional set of calculations were performed for pocket P5 to lower the standard error. The full set of data for each replica with the MBAR and the TI analysis are presented in Tables SI-5 and SI-6.

From the calculations of binding free energies of different replicas for each pocket, we computed the average binding free energy in each pocket. In pocket P7, one data seemed to be an outlier (see Table SI-5 and SI-6), and we have thus performed a Dixon's Q-test statistical analysis to unambiguously identify putative outliers in the data. In such a test, the value  $Q = \text{gap}/\text{range}$  is defined as the ratio between the gap between one value and its closest one, and the range of the values in the series. Q is computed for the highest and the lowest values of a series, and if Q is higher than a tabulated number that depends on the number of data points, then the corresponding value can be considered as an outlier. For example, if we set the confidence at 99% and with five values in the series, if  $Q > 0.821$  then the value must be discarded. From all pockets, only the first value from pocket P7 was found to be an outlier ( $Q=0.845$  with MBAR and  $Q=0.881$  with TI), and the molecular explanation of it is described in SI. Thus, for pocket P7, we have used four data.

Overall the data from MBAR and TI were found to be highly comparable (see Figure SI-23). The average binding free energies from the two analysis methods and the population of each pocket are reported in Figure 5 and in Table SI-4. Three pockets out of the 14 were found to be meaningful: P5, P7 and P13. The computed binding free energies are  $-5.4 \pm 1.1$ ,  $-5.7 \pm 0.1$  and  $-6.1 \pm 0.9$  kcal/mol with MBAR data, and  $-5.2 \pm 0.9$ ,  $-5.4 \pm 0.1$ ,  $-6.1 \pm 0.9$  kcal/mol with TI data.

Experimentally, only the Michaelis constant  $K_M$  of bicarbonate is available with values of 0.10 mM<sup>25</sup> and 0.12 mM<sup>59</sup> reported. One can assume that  $K_d \approx K_M$  (where  $K_d$  is the dissociation constant) and write  $\Delta G_{Binding} \approx -RT \cdot \ln(1/K_M)$  (see SI for a discussion), which leads to binding free energies of -5.5 and -5.4 kcal/mol. Thus, the computed binding free energies of pockets P5 and P7 are within 0.3 kcal/mol to the experimental value with either MBAR or TI, and are within 0.7 kcal/mol for P13. With data from MBAR, the pockets are found to be populated at respectively 15, 24 and 55%, whereas with data from TI they are populated at 15, 20 and 59%. Pocket P3 is populated at 6 and 7% and all the other ones are populated at most 0.1%. From these computational data, we thus conclude that pockets P5, P7 and P13 should be considered as putative binding sites for bicarbonate, with probabilities that are comparable. P13 has the lowest binding free energies, but P5 and P7 have values very close to the experimental one.

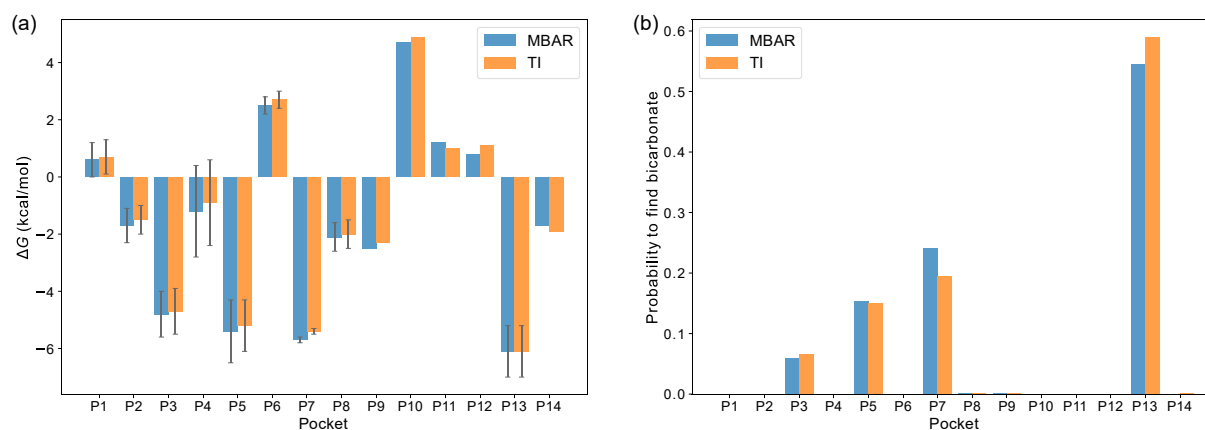


**Figure 5.** (a) Average binding free energies in each pocket with MBAR and TI data. When available, standard errors are reported. (b) Probability to find bicarbonate in each pocket.

As can be seen in Figure 4 and Figure SI-7, pocket P13 is buried inside the protein with a distance between magnesium(II) and bicarbonate of  $\sim 14$  Å. Interactions between the negatively charged bicarbonate and the positively charged Arg610 and Arg641 explain the low binding free energy

for this pocket (see Figure 6). Bicarbonate may serve as an anchor between these two residues to restrict the relative motion between  $\alpha$ -helix 26 (made of residues 610-629) and loop I (made of residues 640-649) and activate the enzyme, without being consumed during the catalytic cycle. A similar behavior occurs with Rubisco, where a lysine must first be activated to a carbamate through a reaction with a  $\text{CO}_2$  molecule, and then the catalytic cycle occurs with the  $\text{CO}_2$  molecules as substrates. The hypothesis of bicarbonate serving as an allosteric activator of PEPC could experimentally be tested by mutating the positions 610 and/or 641 and measuring the Michaelis constants. However, even if bicarbonate can bind in pocket P13, in the following we will not investigate it further because (i) either our hypothesis is true and bicarbonate is itself an allosteric activator in pocket P13: this means that the reactive bicarbonate substrate will bind to pockets P5 or P7 and we can focus on these pockets, (ii) or our hypothesis is wrong and bicarbonate could bind to pocket P13 before a reactive event since it has a lower binding free energy: in such a case, prior the chemical reaction, bicarbonate will first transfer to pockets P5 or P7 and we can focus on these pockets.

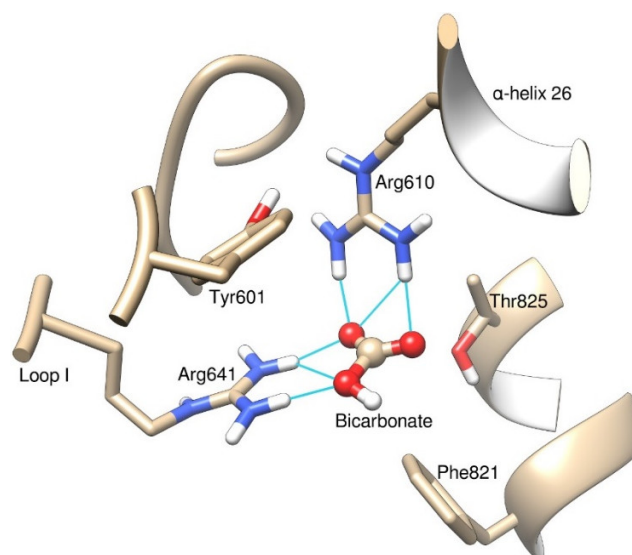


**Figure 6.** Zoom on the position of bicarbonate in pocket P13.

For pockets P5 and P7, two of the free MD simulations where bicarbonate ended in these pockets were extended by 1  $\mu$ s: we didn't observe any exchange between the pockets during the four simulations of 1  $\mu$ s, nor a change of orientation of bicarbonate or a change of interactions with the environment. Pockets P5 and P7 are close to PEP and magnesium, with distances between carbon of bicarbonate and magnesium of 3.0 Å for both, and distances between carbon of bicarbonate and phosphorus of PEP of 5.0 and 4.8 Å respectively. Thus, in these two pockets, the bicarbonate is close to the phosphorus atom of PEP which is beneficial for the reactivity according to the consensus mechanism which involves the formation of a carboxyphosphate intermediate<sup>21,37,39,40</sup>. A cluster analysis was performed on the last 500 ns of the free MD simulations and representative structures are displayed Figure 7 and Figure 8. We observed that the orientation of PEP within the active site is clearly different between pockets P5 and P7, the planes formed by carbons from PEP in each pocket forming an angle of  $\sim 60^\circ$ . The two active sites were found to be very similar, with a very good overlap between the residues. We have only observed a slight shift of position for Asp603 and Lys606, the former being a consequence of the shift of magnesium(II) position. In pocket P5, the magnesium(II) ion is in a square pyramidal geometry, whereas it is in an octahedral environment in pocket P7 (see Figure 7 and Figure 8). In pocket P5, an oxygen atom from bicarbonate is in apical position in the square pyramid, whereas in pocket P7 the same oxygen atom from bicarbonate is in *anti* position from the carboxylate of PEP. In both cases, magnesium(II) interacts with one oxygen from bicarbonate, one oxygen from the carboxylate group of PEP, and with Glu566 and Asp603; the difference between the two coordination structures lies in the interactions with PEP, since in pocket P5 magnesium(II) and PEP interact through one oxygen from the phosphate moiety, whereas in pocket P7 two oxygen atoms from the phosphate moiety are involved. Moreover, in pocket P5, the bicarbonate is stabilized with an

hydrogen bond with the NH from the backbone of Ser602, whereas in pocket P7, the bicarbonate is in the vicinity of three positively-charged residues (Lys606, Arg763, Arg773). Thus, the two pockets are very similar and provide a stabilizing environment for bicarbonate. Mutations on Lys606 and Arg647 were found to affect  $K_M$  of bicarbonate: Lys606 is closer to pocket P7 than P5 by  $\sim 6$  Å, whereas Arg647 is closer to pocket P5 by  $\sim 3$  Å. This means that biochemical data can't be used to decipher the binding sites and sort them.

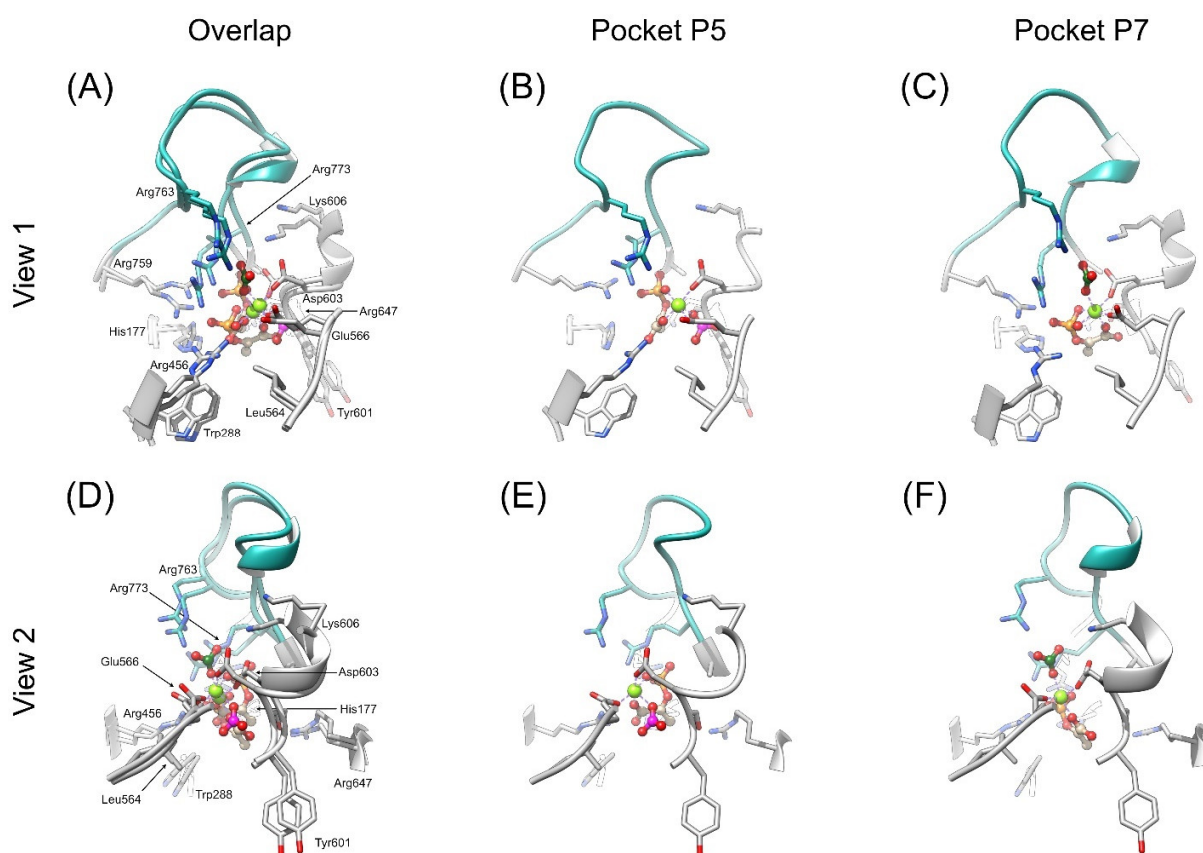


**Figure 7.** Active site of pockets P5 and P7 after alignment on the 29 displayed residues, and seen from two angles. A third view is available in Figure SI-22. Ligands are in spheres, carbons from PEP are in light brown, magnesium is in light green, carbon from bicarbonate in pocket P5 is in pink, carbon from bicarbonate in pocket P7 is in green. The protein is in grey, loop II is in cyan.

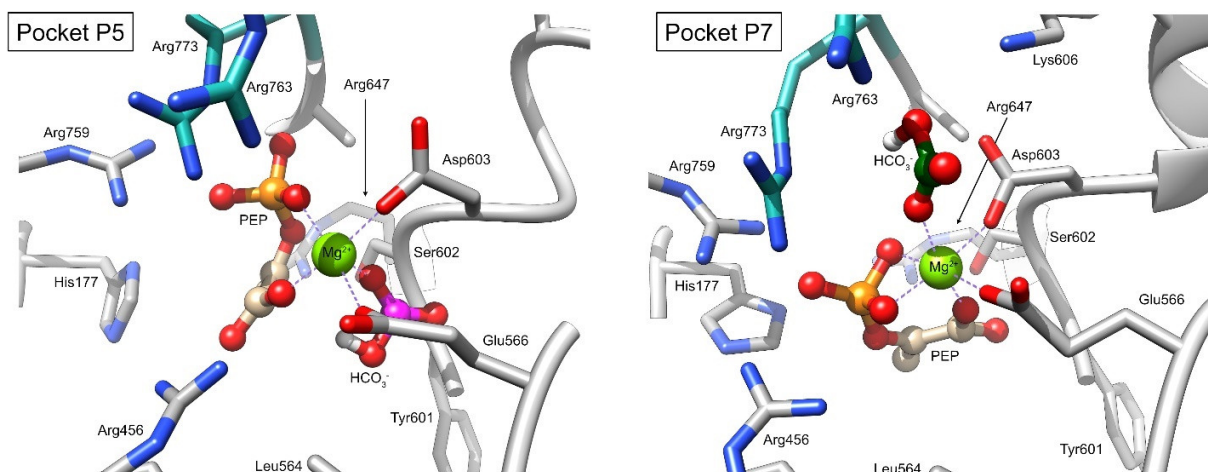


**Figure 8.** Zoom on the active site of pockets P5 and P7. Same color code as in Figure 7.

To compare pockets P5 and P7, we aligned 236 reviewed sequences of PEP Carboxylase which were downloaded from the UniProt website (keeping only those longer than 600 residues). Alignment was made with Clustal Omega provided by EMBL-EBI with default parameters<sup>60</sup>. We found that Lys606 and Arg647 (which are the only two residues which were found to have a meaningful impact on  $K_M$ ) and Arg763 and Arg773 (which interact with bicarbonate in pocket P7) are all conserved in all the sequences. No other residue was found to be a putative probe for deciphering the two pockets. Thus, we couldn't conclude on the preferential binding site of bicarbonate with sequence alignment.

We then turned to mutants of PEPC. Upon mutations of residues Lys762, Arg763 and Arg764 in *E. coli* and maize (which are located on loop II), a side-reaction involving water molecules from solvent occurs, which suggest that loop II cannot protect anymore the active site<sup>21</sup>. Thus, the conformation of loop II is impacted by mutations, and we didn't use mutations made on this loop. Instead, we used data from Dong *et al.* who mutated Lys606<sup>25</sup>; the strongest effect was observed when this residue was mutated to Asn with  $K_M(\text{HCO}_3^-)$  going from 0.10 mM to 2.5 mM, i.e.



binding free energy increasing from -5.5 kcal/mol to -3.6 kcal/mol ( $\Delta\Delta G = +1.9$  kcal/mol). Starting from representative snapshots of pockets P5 and P7, the mutation was performed with UCSF Chimera<sup>44</sup>, the structures were built again (solvation, addition of ions, etc...) and were equilibrated during 500 ns. The same procedure as already described for FEP calculations was then performed (see SI for details). Six snapshots for each pocket were extracted at 500, 490, 480, 400, 390 and 380 ns to start the FEP calculations, and the average binding free energies between the first three and the last three were compared to ensure that comparable values are obtained, meaning that the mutants' structures are well equilibrated. With data from MBAR, we have calculated binding free energies of  $-4.4 \pm 0.7$  kcal/mol for pocket P5 and  $-6.5 \pm 0.7$  kcal/mol for pocket P7, i.e.  $\Delta\Delta G$  of +1.0 and -0.8 kcal/mol respectively. With data from TI, we have calculated binding free energies of  $-4.2 \pm 0.7$  kcal/mol for pocket P5 and  $-6.4 \pm 0.7$  kcal/mol for pocket P7, i.e.  $\Delta\Delta G$  of +1.0 and -1.0 kcal/mol respectively. This provides contradictory results: on one hand, only data for pocket P5 are compatible with the experimental data which found a positive  $\Delta\Delta G$  of +1.9 kcal/mol; on the other hand, binding in the K606N mutant in pocket P7 is stronger by 2.3 kcal/mol than in pocket P5. Thus, we can't conclude yet on the binding site of bicarbonate in PEP Carboxylase. We point out that, as already mentioned, loop II is supposed to be in a closed conformation during the catalytic cycle (acting as a lid) since upon mutations on this loop the activity of a side reaction increased by tenfold<sup>21</sup>, and  $k_{cat}$  and  $K_M(\text{HCO}_3^-)$  respectively decreased and increased. Thus, the experimental binding free energies that we have used here as a comparison were obtained with the loop probably in a closed conformation (since they were derived from  $K_M$ ) whereas our simulations were performed with the open conformation. We are currently working on predicting the closed conformation of loop II, and once it will be found we will replicate the calculations of the binding

free energy of bicarbonate in the two pockets to see if a difference arises. Structures of the system build from 5VYJ with the bicarbonate in pockets P5 or P7 are provided in Zenodo as PDB files.

In the current article, we sought to help finding the binding site of bicarbonate in PEP Carboxylase in order to study in the future questions such as loop motions, allosteric regulation or chemical reactivity. Using non-equilibrium MD simulations (steered-MD), we have identified 14 putative binding sites. The binding free energy of bicarbonate in each site was then precisely computed with alchemical free energy calculations, and we found that three sites are meaningful with computed binding free energies within 1 kcal/mol to experimental values. One site was found to be a candidate for allosteric activation by restricting the motion between an  $\alpha$ -helix and a loop. Neither sequence alignment nor calculations on the mutant K606N allowed to discriminate the two remaining pockets. However, since bicarbonate is a small ligand with not a lot of binding features, we could also envision that it can diffuse and fluctuate between different positions within the active site and we cannot firmly rule out that bicarbonate could bind in both pockets P5 and P7; only experiments will provide a definitive answer, and since the environment in both pockets are very similar only crystallography may be able to provide an answer. Our next study on PEPC will focus on the prediction of the closed conformation of loop II, which may then help to design analogs of PEP that will guide crystallography studies. We will then focus on the allosteric regulation and the phosphorylation of PEPC.

#### ASSOCIATED CONTENT

**Supporting Information.** The following files are available free of charge: presentation of PEP Carboxylase, computational details, discussions on (i) pushing the bicarbonate inside the protein, (ii) the sampling of the active site, (iii) pulling bicarbonate outside the protein, (iv) free energy

perturbations with details on each term of the thermodynamic cycle, the convergence, the outlier, and the corrections due to the charged ligands (PDF). Structure of the enzyme with bicarbonate in pockets P5 and P7 are provided as PDB files, and scripts to perform the corrections of computational artefacts are provided as bash and python scripts, all at the address <https://zenodo.org/doi/10.5281/zenodo.10204297>.

#### AUTHOR INFORMATION

Nicolas Chéron (corresponding author): ORCID: 0000-0002-4090-5897

#### Notes

The authors declare no competing financial interests.

#### ACKNOWLEDGMENT

This work was supported by CNRS, ENS-PSL and Sorbonne Université. The author thanks Julien Henri for fruitful discussions on Calvin-Benson enzymes (Sorbonne Université, Paris), Elise Duboué-Dijon and Jérôme Hénin (IBPC, Paris) for fruitful discussions regarding constraints in free energy calculations and analysis, Daniel Borgis (ENS-PSL, Paris) for fruitful discussions regarding electrostatics, and Damien Laage (ENS-PSL, Paris) for various fruitful scientific discussions. This work was granted access to the HPC resources of CINES and IDRIS under the allocation 2020-077156 made by GENCI.

#### DATA AND SOFTWARE AVAILABILITY

All software used for the current article are open-source and can be obtained through their webpages. All scripts, input files, analysis files are available at the address: <https://zenodo.org/doi/10.5281/zenodo.10204297>.

## REFERENCES

- (1) Bloom, D. E. 7 Billion and Counting. *Science* **2011**, 333 (6042), 562–569. <https://doi.org/10.1126/science.1209290>.
- (2) Sage, R. F.; Sage, T. L.; Kocacinar, F. Photorespiration and the Evolution of C4 Photosynthesis. *Annu. Rev. Plant Biol.* **2012**, 63 (1), 19–47. <https://doi.org/10.1146/annurev-arplant-042811-105511>.
- (3) Raines, C. A.; Harrison, E. P.; Ölçer, H.; Lloyd, J. C. Investigating the Role of the Thiol-Regulated Enzyme Sedoheptulose-1,7-Bisphosphatase in the Control of Photosynthesis. *Physiol. Plant.* **2000**, 110 (3), 303–308. <https://doi.org/10.1111/j.1399-3054.2000.1100303.x>.
- (4) Furbank, R. T.; Hatch, M. D.; Jenkins, C. L. D. C4 Photosynthesis: Mechanism and Regulation. In *Photosynthesis: Physiology and Metabolism*; 2000; pp 435–457.
- (5) Bassham, J. A.; Benson, A. A.; Calvin, Melvin. The Path of Carbon in Photosynthesis. *J. Biol. Chem.* **1950**, 185 (2), 781–787. [https://doi.org/10.1016/S0021-9258\(18\)56368-7](https://doi.org/10.1016/S0021-9258(18)56368-7).
- (6) Lefebvre, S.; Lawson, T.; Fryer, M.; Zakhleniuk, O. V.; Lloyd, J. C.; Raines, C. A. Increased Sedoheptulose-1,7-Bisphosphatase Activity in Transgenic Tobacco Plants Stimulates Photosynthesis and Growth from an Early Stage in Development. *Plant Physiol.* **2005**, 138 (1), 451–460. <https://doi.org/10.1104/pp.104.055046>.
- (7) Simkin, A. J.; Lopez-Calcano, P. E.; Davey, P. A.; Headland, L. R.; Lawson, T.; Timm, S.; Bauwe, H.; Raines, C. A. Simultaneous Stimulation of Sedoheptulose 1,7-Bisphosphatase, Fructose 1,6-Bisphosphate Aldolase and the Photorespiratory Glycine Decarboxylase-H Protein Increases CO<sub>2</sub> Assimilation, Vegetative Biomass and Seed Yield in Arabidopsis. *Plant Biotechnol. J.* **2017**, 15 (7), 805–816. <https://doi.org/10.1111/pbi.12676>.
- (8) Hammel, A.; Sommer, F.; Zimmer, D.; Stitt, M.; Mühlhaus, T.; Schroda, M. Overexpression of Sedoheptulose-1,7-Bisphosphatase Enhances Photosynthesis in *Chlamydomonas Reinhardtii* and Has No Effect on the Abundance of Other Calvin-Benson Cycle Enzymes. *Front. Plant Sci.* **2020**, 11.
- (9) Qu, Y.; Sakoda, K.; Fukayama, H.; Kondo, E.; Suzuki, Y.; Makino, A.; Terashima, I.; Yamori, W. Overexpression of Both Rubisco and Rubisco Activase Rescues Rice Photosynthesis and Biomass under Heat Stress. *Plant Cell Environ.* **2021**, 44 (7), 2308–2320. <https://doi.org/10.1111/pce.14051>.
- (10) Meloni, M.; Fanti, S.; Tedesco, D.; Gurrieri, L.; Trost, P.; Fermani, S.; Lemaire, S. D.; Zaffagnini, M.; Henri, J. Structural and Functional Characterization of Chloroplast Ribulose-5-Phosphate-3-Epimerase from the Model Green Microalga *Chlamydomonas Reinhardtii*. *bioRxiv* September 30, 2022, p 2022.09.29.510120. <https://doi.org/10.1101/2022.09.29.510120>.
- (11) Tcherkez, G. G. B.; Farquhar, G. D.; Andrews, T. J. Despite Slow Catalysis and Confused Substrate Specificity, All Ribulose Bisphosphate Carboxylases May Be Nearly Perfectly Optimized. *Proc. Natl. Acad. Sci.* **2006**, 103 (19), 7246–7251. <https://doi.org/10.1073/pnas.0600605103>.
- (12) Bathellier, C.; Tcherkez, G.; Lorimer, G. H.; Farquhar, G. D. Rubisco Is Not Really so Bad: Rubisco Efficiency. *Plant Cell Environ.* **2018**, 41 (4), 705–716. <https://doi.org/10.1111/pce.13149>.
- (13) Endo, T.; Mihara, Y.; Furumoto, T.; Matsumura, H.; Kai, Y.; Izui, K. Maize C4-Form Phosphoenolpyruvate Carboxylase Engineered to Be Functional in C3 Plants: Mutations for

- Diminished Sensitivity to Feedback Inhibitors and for Increased Substrate Affinity. *J. Exp. Bot.* **2008**, *59* (7), 1811–1818. <https://doi.org/10.1093/jxb/ern018>.
- (14) Kellogg, E. A. C4 Photosynthesis. *Curr. Biol.* **2013**, *23* (14), R594–R599. <https://doi.org/10.1016/j.cub.2013.04.066>.
  - (15) Ranum, P.; Peña-Rosas, J. P.; Garcia-Casal, M. N. Global Maize Production, Utilization, and Consumption. *Ann. N. Y. Acad. Sci.* **2014**, *1312* (1), 105–112. <https://doi.org/10.1111/nyas.12396>.
  - (16) Schmer, M. R.; Vogel, K. P.; Mitchell, R. B.; Perrin, R. K. Net Energy of Cellulosic Ethanol from Switchgrass. *Proc. Natl. Acad. Sci.* **2008**, *105* (2), 464–469. <https://doi.org/10.1073/pnas.0704767105>.
  - (17) von Caemmerer, S.; Furbank, R. T. Modeling C4 Photosynthesis. In *C4 Plant Biology*; Elsevier, 1999; pp 173–211. <https://doi.org/10.1016/B978-012614440-6/50007-0>.
  - (18) O’Leary, B.; Park, J.; Plaxton, W. C. The Remarkable Diversity of Plant PEPC (Phosphoenolpyruvate Carboxylase): Recent Insights into the Physiological Functions and Post-Translational Controls of Non-Photosynthetic PEPCs. *Biochem. J.* **2011**, *436* (1), 15–34. <https://doi.org/10.1042/BJ20110078>.
  - (19) Furbank, R. T.; von Caemmerer, S.; Sheehy, J.; Edwards, G. C4 Rice: A Challenge for Plant Phenomics. *Funct. Plant Biol.* **2009**, *36* (11), 845. <https://doi.org/10.1071/FP09185>.
  - (20) Luo, S.; Diehl, C.; He, H.; Bae, Y.; Klose, M.; Claus, P.; Cortina, N. S.; Fernandez, C. A.; Schulz-Mirbach, H.; McLean, R.; Ramírez Rojas, A. A.; Schindler, D.; Paczia, N.; Erb, T. J. Construction and Modular Implementation of the THETA Cycle for Synthetic CO2 Fixation. *Nat. Catal.* **2023**, *6* (12), 1228–1240. <https://doi.org/10.1038/s41929-023-01079-z>.
  - (21) Izui, K.; Matsumura, H.; Furumoto, T.; Kai, Y. Phosphoenolpyruvate Carboxylase: A New Era of Structural Biology. *Annu. Rev. Plant Biol.* **2004**, *55* (1), 69–84. <https://doi.org/10.1146/annurev.arplant.55.031903.141619>.
  - (22) Janc, J. W.; Urbauer, J. L.; O’Leary, M. H.; Cleland, W. W. Mechanistic Studies of Phosphoenolpyruvate Carboxylase from Zea Mays with (Z)- and (E)-3-Fluorophosphoenolpyruvate as Substrates. *Biochemistry* **1992**, *31* (28), 6432–6440. <https://doi.org/10.1021/bi00143a011>.
  - (23) Matsumura, H.; Xie, Y.; Shirakata, S.; Inoue, T.; Yoshinaga, T.; Ueno, Y.; Izui, K.; Kai, Y. Crystal Structures of C4 Form Maize and Quaternary Complex of E. Coli Phosphoenolpyruvate Carboxylases. *Structure* **2002**, *10* (12), 1721–1730. [https://doi.org/10.1016/S0969-2126\(02\)00913-9](https://doi.org/10.1016/S0969-2126(02)00913-9).
  - (24) Kai, Y.; Matsumura, H.; Inoue, T.; Terada, K.; Nagara, Y.; Yoshinaga, T.; Kihara, A.; Tsumura, K.; Izui, K. Three-Dimensional Structure of Phosphoenolpyruvate Carboxylase: A Proposed Mechanism for Allosteric Inhibition. *Proc. Natl. Acad. Sci.* **1999**, *96* (3), 823–828. <https://doi.org/10.1073/pnas.96.3.823>.
  - (25) Dong, L.-Y.; Ueno, Y.; Hata, S.; Izui, K. Effects of Site-Directed Mutagenesis of Conserved Lys606 Residue on Catalytic and Regulatory Functions of Maize C4-Form Phosphoenolpyruvate Carboxylase. *Plant Cell Physiol.* **1997**, *38* (12), 1340–1345. <https://doi.org/10.1093/oxfordjournals.pcp.a029127>.
  - (26) Gao, Y.; Woo, K. c. Site-Directed Mutagenesis of Lys600 in Phosphoenolpyruvate Carboxylase of Flaveria Trinervia: Its Roles in Catalytic and Regulatory Functions. *FEBS Lett.* **1995**, *375* (1–2), 95–98. [https://doi.org/10.1016/0014-5793\(95\)01189-L](https://doi.org/10.1016/0014-5793(95)01189-L).

- (27) Yano, M.; Terada, K.; Umiji, K.; Izui, K. Catalytic Role of an Arginine Residue in the Highly Conserved and Unique Sequence of Phosphoenolpyruvate Carboxylase. *J. Biochem. (Tokyo)* **1995**, *117* (6), 1196–1200. <https://doi.org/10.1093/oxfordjournals.jbchem.a124844>.
- (28) DiMario, R. J.; Cousins, A. B. A Single Serine to Alanine Substitution Decreases Bicarbonate Affinity of Phosphoenolpyruvate Carboxylase in *C4Flaveria Trinervia*. *J. Exp. Bot.* **2019**, *70* (3), 995–1004. <https://doi.org/10.1093/jxb/ery403>.
- (29) Gao, Y.; Woo, K. c. Site-Directed Mutagenesis of *Flaveria Trinervia* Phosphoenolpyruvate Carboxylase: Arg450 and Arg767 Are Essential for Catalytic Activity and Lys829 Affects Substrate Binding. *FEBS Lett.* **1996**, *392* (3), 285–288. [https://doi.org/10.1016/0014-5793\(96\)00832-0](https://doi.org/10.1016/0014-5793(96)00832-0).
- (30) Chen, Z.; Bommareddy, R. R.; Frank, D.; Rappert, S.; Zeng, A.-P. Dereglulation of Feedback Inhibition of Phosphoenolpyruvate Carboxylase for Improved Lysine Production in *Corynebacterium Glutamicum*. *Appl. Environ. Microbiol.* **2014**, *80* (4), 1388–1393. <https://doi.org/10.1128/AEM.03535-13>.
- (31) Takeya, M.; Hirai, M. Y.; Osanai, T. Allosteric Inhibition of Phosphoenolpyruvate Carboxylases Is Determined by a Single Amino Acid Residue in Cyanobacteria. *Sci. Rep.* **2017**, *7* (1), 41080. <https://doi.org/10.1038/srep41080>.
- (32) Tcherkez, G. Modelling the Reaction Mechanism of Ribulose-1,5-Bisphosphate Carboxylase/Oxygenase and Consequences for Kinetic Parameters. *Plant Cell Environ.* **2013**, *36* (9), 1586–1596. <https://doi.org/10.1111/pce.12066>.
- (33) Ngan, C.-H.; Hall, D. R.; Zerbe, B.; Grove, L. E.; Kozakov, D.; Vajda, S. FTSite: High Accuracy Detection of Ligand Binding Sites on Unbound Protein Structures. *Bioinformatics* **2012**, *28* (2), 286–287. <https://doi.org/10.1093/bioinformatics/btr651>.
- (34) Jiménez, J.; Doerr, S.; Martínez-Rosell, G.; Rose, A. S.; De Fabritiis, G. DeepSite: Protein-Binding Site Predictor Using 3D-Convolutional Neural Networks. *Bioinformatics* **2017**, *33* (19), 3036–3042. <https://doi.org/10.1093/bioinformatics/btx350>.
- (35) Le Guilloux, V.; Schmidtke, P.; Tuffery, P. Fpocket: An Open Source Platform for Ligand Pocket Detection. *BMC Bioinformatics* **2009**, *10* (1), 168. <https://doi.org/10.1186/1471-2105-10-168>.
- (36) Tian, W.; Chen, C.; Lei, X.; Zhao, J.; Liang, J. CASTp 3.0: Computed Atlas of Surface Topography of Proteins. *Nucleic Acids Res.* **2018**, *46* (W1), W363–W367. <https://doi.org/10.1093/nar/gky473>.
- (37) Chollet, R.; Vidal, J.; O’Leary, M. H. Phosphoenolpyruvate Carboxylase: A Ubiquitous, Highly Regulated Enzyme in Plants. *Annu. Rev. Plant Physiol. Plant Mol. Biol.* **1996**, *47* (1), 273–298. <https://doi.org/10.1146/annurev.arplant.47.1.273>.
- (38) Vidal, J.; Chollet, R. Regulatory Phosphorylation of *C4* PEP Carboxylase. *Trends Plant Sci.* **1997**, *2* (6), 230–237.
- (39) Kai, Y.; Matsumura, H.; Izui, K. Phosphoenolpyruvate Carboxylase: Three-Dimensional Structure and Molecular Mechanisms. *Arch. Biochem. Biophys.* **2003**, *414* (2), 170–179. [https://doi.org/10.1016/S0003-9861\(03\)00170-X](https://doi.org/10.1016/S0003-9861(03)00170-X).
- (40) Lepiniec, L.; Thomas, M.; Vidal, J. From Enzyme Activity to Plant Biotechnology: 30 Years of Research on Phosphoenolpyruvate Carboxylase. *Plant Physiol. Biochem.* **2003**, *41* (6–7), 533–539. [https://doi.org/10.1016/S0981-9428\(03\)00069-X](https://doi.org/10.1016/S0981-9428(03)00069-X).
- (41) Mancera, R. L.; Carrington, B. J. The Molecular Binding Interactions of Inhibitors and Activators of Phosphoenolpyruvate Carboxylase. *J. Mol. Struct. THEOCHEM* **2005**, *755* (1–3), 151–159. <https://doi.org/10.1016/j.theochem.2005.08.014>.

- (42) González-Segura, L.; Mújica-Jiménez, C.; Juárez-Díaz, J. A.; Güemez-Toro, R.; Martínez-Castilla, L. P.; Muñoz-Clares, R. A. Identification of the Allosteric Site for Neutral Amino Acids in the Maize C4 Isozyme of Phosphoenolpyruvate Carboxylase: The Critical Role of Ser-100. *J. Biol. Chem.* **2018**, *293* (26), 9945–9957. <https://doi.org/10.1074/jbc.RA118.002884>.
- (43) Muñoz-Clares, R. A.; González-Segura, L.; Juárez-Díaz, J. A.; Mújica-Jiménez, C. Structural and Biochemical Evidence of the Glucose 6-Phosphate-Allosteric Site of Maize C4-Phosphoenolpyruvate Carboxylase: Its Importance in the Overall Enzyme Kinetics. *Biochem. J.* **2020**, *477* (11), 2095–2114. <https://doi.org/10.1042/BCJ20200304>.
- (44) Pettersen, E. F.; Goddard, T. D.; Huang, C. C.; Couch, G. S.; Greenblatt, D. M.; Meng, E. C.; Ferrin, T. E. UCSF Chimera--a Visualization System for Exploratory Research and Analysis. *J. Comput. Chem.* **2004**, *25* (13), 1605–1612. <https://doi.org/10.1002/jcc.20084>.
- (45) Webb, B.; Sali, A. Comparative Protein Structure Modeling Using MODELLER. *Curr. Protoc. Bioinforma.* **2016**, *54* (1), 5.6.1–5.6.37. <https://doi.org/10.1002/cpbi.3>.
- (46) Shen, M.; Sali, A. Statistical Potential for Assessment and Prediction of Protein Structures. *Protein Sci.* **2006**, *15* (11), 2507–2524. <https://doi.org/10.1110/ps.062416606>.
- (47) Tovar-Méndez, A.; Mújica-Jiménez, C.; Muñoz-Clares, R. A. Physiological Implications of the Kinetics of Maize Leaf Phosphoenolpyruvate Carboxylase. *Plant Physiol.* **2000**, *123* (1), 149–160. <https://doi.org/10.1104/pp.123.1.149>.
- (48) Briones, R.; Blau, C.; Kutzner, C.; de Groot, B. L.; Aponte-Santamaría, C. GROmaps: A GROMACS-Based Toolset to Analyze Density Maps Derived from Molecular Dynamics Simulations. *Biophys. J.* **2019**, *116* (1), 4–11. <https://doi.org/10.1016/j.bpj.2018.11.3126>.
- (49) Jorgensen, W. L.; Thomas, L. L. Perspective on Free-Energy Perturbation Calculations for Chemical Equilibria. *J. Chem. Theory Comput.* **2008**, *4* (6), 869–876. <https://doi.org/10.1021/ct800011m>.
- (50) Mobley, D. L.; Klimovich, P. V. Perspective: Alchemical Free Energy Calculations for Drug Discovery. *J. Chem. Phys.* **2012**, *137* (23), 230901. <https://doi.org/10.1063/1.4769292>.
- (51) Chipot, C. Frontiers in Free-Energy Calculations of Biological Systems. *WIREs Comput. Mol. Sci.* **2014**, *4* (1), 71–89. <https://doi.org/10.1002/wcms.1157>.
- (52) Cournia, Z.; Allen, B.; Sherman, W. Relative Binding Free Energy Calculations in Drug Discovery: Recent Advances and Practical Considerations. *J. Chem. Inf. Model.* **2017**, *57* (12), 2911–2937. <https://doi.org/10.1021/acs.jcim.7b00564>.
- (53) Mobley, D. L.; Gilson, M. K. Predicting Binding Free Energies: Frontiers and Benchmarks. *Annu. Rev. Biophys.* **2017**, *46* (1), 531–558. <https://doi.org/10.1146/annurev-biophys-070816-033654>.
- (54) Mey, A. S. J. S.; Allen, B. K.; Macdonald, H. E. B.; Chodera, J. D.; Hahn, D. F.; Kuhn, M.; Michel, J.; Mobley, D. L.; Naden, L. N.; Prasad, S.; Rizzi, A.; Scheen, J.; Shirts, M. R.; Tresadern, G.; Xu, H. Best Practices for Alchemical Free Energy Calculations. *Living J. Comput. Mol. Sci.* **2020**, *2* (1), 18378. <https://doi.org/10.33011/livecoms.2.1.18378>.
- (55) Song, L. F.; Merz, K. M. Jr. Evolution of Alchemical Free Energy Methods in Drug Discovery. *J. Chem. Inf. Model.* **2020**, *60* (11), 5308–5318. <https://doi.org/10.1021/acs.jcim.0c00547>.
- (56) Shirts, M. R.; Chodera, J. D. Statistically Optimal Analysis of Samples from Multiple Equilibrium States. *J. Chem. Phys.* **2008**, *129* (12), 124105. <https://doi.org/10.1063/1.2978177>.

- (57) Rocklin, G. J.; Mobley, D. L.; Dill, K. A.; Hünenberger, P. H. Calculating the Binding Free Energies of Charged Species Based on Explicit-Solvent Simulations Employing Lattice-Sum Methods: An Accurate Correction Scheme for Electrostatic Finite-Size Effects. *J. Chem. Phys.* **2013**, *139* (18), 184103. <https://doi.org/10.1063/1.4826261>.
- (58) Lin, Y.-L.; Aleksandrov, A.; Simonson, T.; Roux, B. An Overview of Electrostatic Free Energy Computations for Solutions and Proteins. *J. Chem. Theory Comput.* **2014**, *10* (7), 2690–2709. <https://doi.org/10.1021/ct500195p>.
- (59) Muramatsu, M.; Suzuki, R.; Yamazaki, T.; Miyao, M. Comparison of Plant-Type Phospho Enol Pyruvate Carboxylases from Rice: Identification of Two Plant-Specific Regulatory Regions of the Allosteric Enzyme. *Plant Cell Physiol.* **2015**, *56* (3), 468–480. <https://doi.org/10.1093/pcp/pcu189>.
- (60) Madeira, F.; Pearce, M.; Tivey, A. R. N.; Basutkar, P.; Lee, J.; Edbali, O.; Madhusoodanan, N.; Kolesnikov, A.; Lopez, R. Search and Sequence Analysis Tools Services from EMBL-EBI in 2022. *Nucleic Acids Res.* **2022**, *50* (W1), W276–W279. <https://doi.org/10.1093/nar/gkac240>.



## TOC GRAPHICS

